Journal of Nuclear Materials 509 (2018) 1–8

Contents lists available at ScienceDirect

Journal of Nuclear Materials

journal homepage: www.elsevier.com/locate/jnucmat

Microstructural characterization of as-fabricated and irradiated U-Mo fuel using SEM/EBSD

Daniel Jadernas*, Jian Gan, Dennis Keiser, James Madden, Mukesh Bachhav, Jan-Fong Jue, Adam Robinson

Idaho National Laboratory, Materials and Fuels complex, 2525 Fremont Ave, Idaho Falls, ID, 83402, USA

HIGHLIGHTS

- Electron backscatter diffraction (EBSD) was successfully used to study irradiated U-Mo nuclear fuel particles.
- Grain orientation and grain boundary characteristics data were collected comparing unirradiated and irradiated U-Mo fuel.
- EBSD data suggest that the subgrains formation mechanism during irradiation is polygonization rather than recrystallization.

GRAPHICAL ABSTRACT

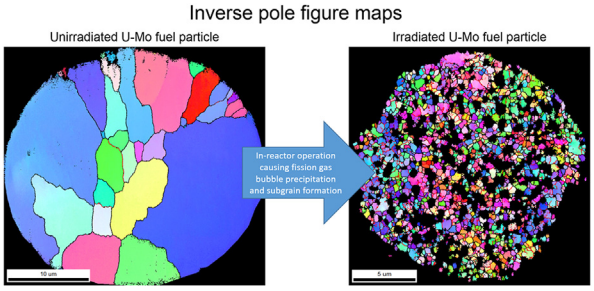

ARTICLE INFO

Article history:
Received 21 March 2018
Received in revised form
5 June 2018
Accepted 6 June 2018
Available online 7 June 2018

Keywords:
U-Mo
Nuclear fuel
Neutron irradiation
SEM
EBSD
Subgrain formation
Polygonization

ABSTRACT

Electron Backscattered Diffraction (EBSD) is an effective technique for revealing many details about the microstructure of materials, e.g. crystallographic orientation, grain size, grain boundary properties, texture, intragranular misorientation, and subgrain formation. Since these details are of interest for improving the irradiation performance understanding of any irradiated nuclear fuel (e.g. swelling behavior), this technique has been applied successfully on U-7 wt% Mo before and after irradiation. This fuel is a high-density, low-enriched uranium fuel currently being developed for application in research and test reactors. Based on the results of this characterization, it was found that when as-fabricated U-7 wt% Mo is irradiated to around 5.3×10^{21} fissions/cm^3 the original large grains (diameter ~4 μm) are subdivided into much smaller grains (diameter ~0.3 μm) and most of these subdivided grain boundaries are low angle boundaries. The EBSD analysis suggests that the grain subdivision in the irradiated U-7 wt% Mo was driven by polygonization, not recrystallization as defined by classic metallurgy as a result of heavy cold work followed by heat treatment.

1. Introduction

The program to convert research and test reactors from the use of highly enriched uranium to low enriched uranium ($U^{235} < 20\%$) started under the U.S. Department of Energy in 1978. Since then developing nuclear fuels with lower enrichment has been a global effort [1]. Several fuel materials have been developed for this purpose and different metallic uranium alloy fuel types are promising options. These metallic alloys increase the fissile material density compared to other fuel types while maintaining a low enrichment enabling reactors to operate at specified power after conversion from high to low enriched fuel [2]. The cubic γ-U, stable at

* Corresponding author.
E-mail address: daniel.jadernas@inl.gov (D. Jadernas).

https://doi.org/10.1016/j.jnucmat.2018.06.007
0022-3115/

temperatures above 770 °C, has shown promising results during in-pile irradiation while the low temperature orthorhombic α-phase behaves less predictable [3]. To stabilize the γ-U phase down to room temperature alloying elements are added [4,5]. Molybdenum has shown to stabilize the γ-U phase and one candidate fuel type that has shown promising results during irradiation in test reactors is the U-7 wt% Mo dispersion fuel consisting of fuel particles embedded in an Al alloy matrix and cladding material. To mitigate fuel particle to matrix interaction during operation that can affect fuel swelling negatively, Si can be added to the Al fuel meat matrix suppressing the interaction layer and stabilizing the fuel swelling behavior [6,7].

It is of key importance to mitigate extensive dimensional changes during irradiation. This requires having control over the fuel meat swelling during in-reactor service. One of the parameters controlling the amount of swelling is the fuel microstructure. The as-fabricated fuel microstructure will affect the evolution of the fuel microstructure during irradiation and therefore also affect the fuel swelling and dimensional change of the fuel plate. During irradiation, subgrains can form at high burnups ($>3 \times 10^{21}$ fissions/cm^3) that can lead to enhanced growth of fission gas bubbles, which can accelerate swelling of the fuel [8,9].

The work in this paper investigates the microstructural changes that occur during irradiation of U-7 wt% Mo dispersion fuel by utilizing an electron backscatter diffraction apparatus (EBSD) coupled with a focused ion beam equipped scanning electron microscope (FIB/SEM) to characterize the as-fabricated U-7 wt% Mo fuel microstructure as well as U-7 wt% Mo fuel irradiated in the advanced test reactor (ATR) at the Idaho National Laboratory (INL) [10].

EBSD is a tool that has not been extensively used for irradiated nuclear fuel material but can reveal many details about the microstructure that have not been observed before [11], e.g. crystallographic orientation, grain size, grain boundary properties, texture, intragranular misorientation, and subgrain formation etc. EBSD has previously been used to study unirradiated U-7 wt% Mo fuel [12,13] but this is the first time the technique has been employed to the irradiated U-Mo fuel material.

The purpose of the work presented in this paper was twofold; (1) developing a technique to study irradiated U-Mo fuel using EBSD, and (2) to gain more understanding regarding the subgrain formation occurring during in-reactor irradiation. Changes in microstructure during irradiation will affect the swelling of the fuel and therefore requires further understanding. Possibly mitigating this effect can increase the fuel's reliability [14].

2. Experimental details

The as-fabricated sample (JJ-652) and irradiated sample (KGT-2141) came from fuel plates fabricated as part of the AFIP-1 irradiation experiment [15], and sample characteristics are listed in Table 1. Fig. 1 shows a schematic diagram of the microstructure for these samples, where U-7 wt% Mo particles are dispersed in an Al-4043 matrix. Ref. [8] describes how this fuel was fabricated. Samples for characterization were prepared using standard metallographic techniques, where sample cross-sections were sliced from the fuel plates and embedded in epoxy resin mounts, which were then cured and ground using SiC papers with grit sizes 320 (35 μm), 600 (15 μm), 800 (13 μm), 1200 (8 μm). The first grinding step is performed to produce a flat specimen. The duration of the subsequent steps were 5 min each. The final SiC grinding step is followed by two polishing steps using diamond suspensions (3 μm and 1 μm) together with polishing cloths for 5 min each. A final polishing step was employed using vibratory polishing in 0.04 μm colloidal Silica suspension for 2 h. The samples were thoroughly rinsed in water between the different grinding/polishing steps and cleaned in ethanol when finished.

Surface preparation is critical for a high quality EBSD analysis since the signal is mainly produced from the absolute surface layers of the material [13]. It is always a challenge to produce a scratch free surface through mechanical polishing for highly radioactive irradiated fuels. During initial EBSD characterization, the Kikuchi pattern confidence index (measures how well the patterns can be indexed and fitted to a specific crystal structure) was observed to be very poor in the as-polished condition. The reason for this was most likely due to either the residual mechanical damage or the development of a surface oxide on the sample surface before insertion into the SEM vacuum chamber, which caused distortion of the generated Kikuchi patterns. Similar problems have been reported for unirradiated U-Mo alloys previously [12].

In order to improve the sample surface conditions and confidence index during the EBSD measurements the FIB was used to polish the surface in-situ in the vacuum chamber. An FEI Quanta 3D FEG FIB/SEM Ga ion source instrument was employed at an ion acceleration voltage of 30 kV and the sample was oriented in the vacuum chamber so that the ion beam would impinge on the samples surface at a ~1° glancing angle, see schematic of the setup in Fig. 2a. The working distance used for all work was 10 mm and the final surface was polished using a 1 nA Ga ion probe at 30 kV. This may seem as a high current and voltage to use as the final step of polishing the surface but these parameters gave the best end result. Attempts were made cleaning the surface using lower acceleration voltages, as well as using lower probe currents. However, the extended polishing time increased the amount of curtaining, especially for the irradiated sample containing a lot of bubbles. Furthermore, low ion energy cleaning was also not successful, potentially due to the additional Ga ion dose received to the sample surface in combination with less sputtering from the sample surface.

Ion milling in FIB could affect the surface quality for EBSD analysis by introducing vacancies and implantation of Ga. To estimate the impact of the Ga ion-sample surface interactions TRIM (TRansport of Ions in Matter) calculations were performed using the SRIM (the Stopping and Range of Ions in Matter) suite of software [16]. For the calculations, 50000 Ga + ions were simulated to hit the U-7 wt% Mo target material having a density of 17.3 g/cm^3. The “Quick” Kinchin and Pease option was used in the SRIM calculation to most accurately study the collisional damage to the sample [17]. Two different ion incidence angles were used for the calculations; 0° (normal) and 89° (glancing). The amount of

Table 1
Characteristics of analyzed samples.

Sample name	Cladding material	Fuel material	Calculated beginning of life centerline temperature [°C]	Calculated Local Fuel Particle Fission Density [fissions/cm^3]
JJ-652	Al-6061	U-7wt% Mo in Al-4043[a] matrix	n/a	n/a
KGT-2141	Al-6061	U-7wt% Mo in Al-4043[a] matrix	138	5.3×10^{21} (13 %FIMA[b])

[a] Al-4043 has a nominal composition (in wt-%) of 4.5Si-0.8Fe-0.3Cu-0.05Mn-0.05Mg-0.1Zn-0.2Ti-0.0008Be-Bal Al.
[b] %FIMA: percent initial heavy metal atoms that have undergone fission.

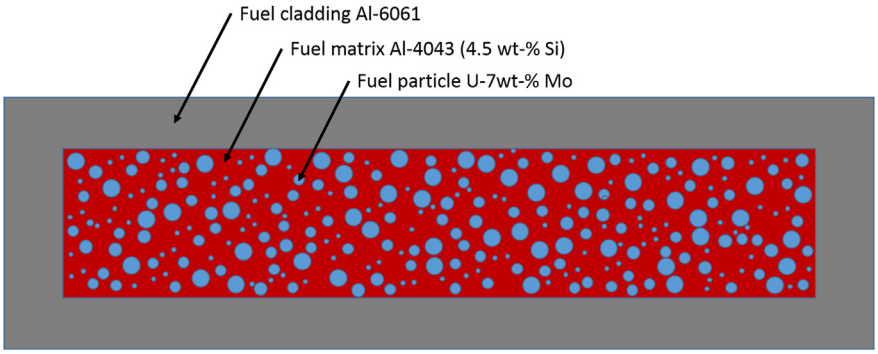

Fig. 1. Axial cross section schematic of a U-7 wt% Mo dispersion fuel plate.

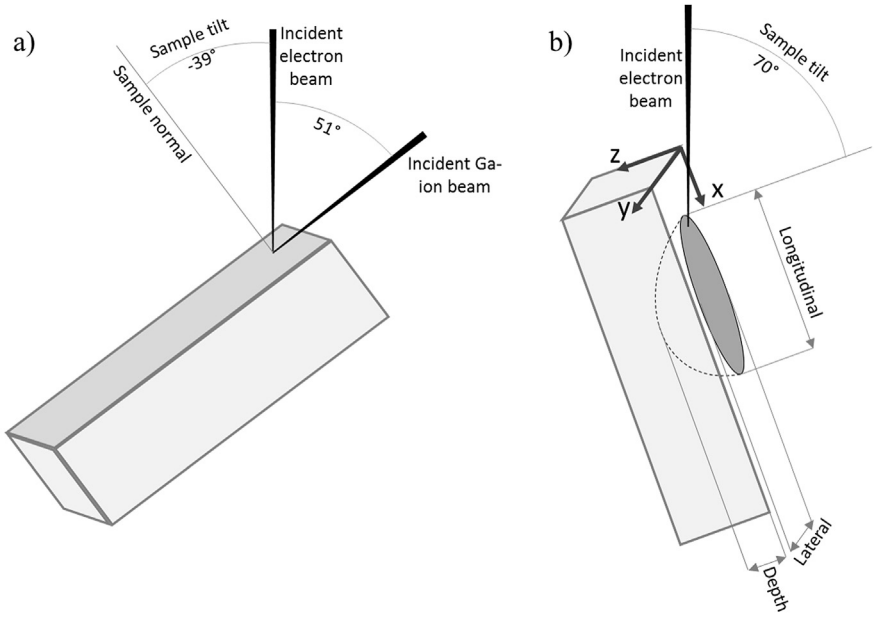

Fig. 2. The setup used during a) Ga ion surface reconditioning and polishing and b) EBSD measurements.

implanted Ga ions was also calculated for the two cases as this may also impact the crystal structure in the sample. All these calculations assume that no sputtering occurs from the sample surface during the FIB milling. Taking this factor into account would probably decrease the impact of the ion irradiation on the vacancy generation and Ga ion implantation.

The same FIB/SEM instrument described above is also equipped with the Trident system supplied by EDAX including energy and wavelength dispersive x-ray spectrometers as well as a DigiView EBSD camera. For these measurements 8 × 8 pixels were binned for the 14 megapixel EBSD camera. The camera and processing system was capable of indexing up to 200 Kikuchi patterns per second. The acquisition software used was TEAM version 4.4 and the data analysis was done with OIM Analysis 8 with neighbor patterns averaging (NPAR) capabilities [18]. All EBSD measurements were performed with the sample tilted at 70° towards the EBSD detector. For the present work, an electron acceleration voltage and current of 30 kV and 48 nA, respectively, were used. This relatively high beam current was used to increase the Kikuchi pattern intensity on the fluorescent screen of the EBSD detector and the acceleration voltage was chosen for the measurements to be less sensitive to surface defect/contamination. The raster step size used during the EBSD measurements was 50 nm at a speed of around 100 patterns per second and the raster pattern used was hexagonal. The 50 nm step size used in this work pushes the limit to what is achievable in terms of resolution using the conventional EBSD technique for a material with this density at this electron acceleration voltage. A schematic showing the setup is presented in Fig. 2b.

3. Results and discussion

3.1. Sample surface reconditioning using the FIB

SEM micrographs comparing the unirradiated and the irradiated fuel sample before any surface reconditioning are shown in Fig. 3. The overview micrographs in the upper row of Fig. 3 show the general fuel structure, where the fuel cladding, fuel particles and fuel-matrix-interaction layers are shown. Other observations are that the interaction layer increases in thickness during irradiation and the fuel swelling during irradiation is significant. The detailed images, in the lower row in Fig. 3, show fuel particles in some more detail. During irradiation, fission products are generated as a result of fissions and eventually fission gas bubbles will precipitate and grow, as observed in the micrograph of the irradiated sample. In this mechanically polished state, very poor Kikuchi patterns could be generated from the sample. As mentioned earlier, this is

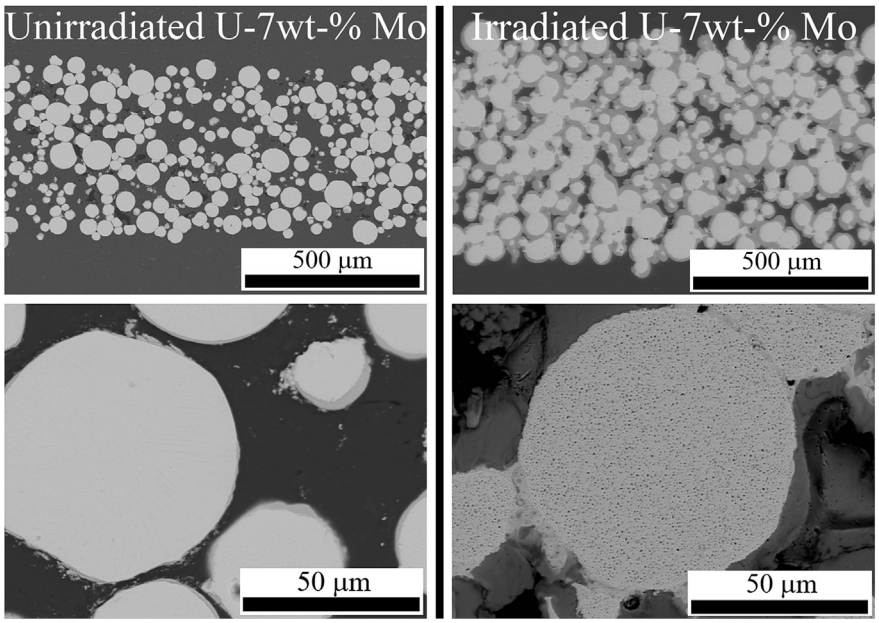

Fig. 3. SEM backscattered electron micrographs from the unirradiated and irradiated fuel sample JJ-652 and KGT-2141, respectively. Upper row shows an overview and the lower row reveals more details of the fuel particles. The U-7Mo fuel particles are bright grey, the interaction layer is medium grey, and the matrix is dark.

attributed either to the fact that U-7 wt% Mo particles are easily oxidized and form an oxide film distorting the patterns or that deformation not visible during imaging in the SEM is still present. It should be noted that several irradiated samples have been analyzed and only poor and sporadic Kikuchi patterns could be generated from these samples without surface reconditioning using the FIB.

The sample surface reconditioning using the FIB will affect the sample surface layer by ion implantation and defect generation. Since EBSD is a very surface sensitive method, it is very important to minimize the detrimental effects of the Ga ion-sample interaction on the sample surface quality. TRIM calculations were made to optimize the experimental setup during the FIB surface reconditioning. The calculated vacancy generation using normal incidence and glancing incidence ions as a function sample depth is shown in Fig. 4a. The vacancy generation is plotted as the amount of vacancies generated per Ga ion per Angstrom the ion penetrates the sample. Normal incidence Ga ions generate on average 352 while the glancing angle ions only generate on average 106 vacancies per ion (calculated as the area under the graph in Fig. 4a). The total affected depth is also almost half comparing the glancing incidence to the normal incidence case (20 nm compared to 30–40 nm). Furthermore, the magnitude of the damage is high in the absolute surface for the glancing incident case (≤2 nm) but is thereafter significantly lower than the normal incidence case resulting in that FIB surface reconditioning was performed using a glancing incidence ion angle. This was also verified since surface reconditioning at incidence angles $\gg 1^{\circ}$ resulted in very poor EBSD pattern indexing success rate rendering the measurements useless. The injected Ga ions at high incidence angle are also expected to have a negative effect on the EBSD measurement. Fig. 4b shows that glancing angle ion milling results in less than 1/4 of the injected Ga ions compared to the normal incidence case (calculated as the area under the graph in Fig. 4b). This assumes that the total Ga ion dose in atoms/cm^2 is the same in the two cases. Similar sample depths are affected by Ga implantation as for the vacancy generation. Sputtering of the sample surface is not considered during TRIM calculations. Since the Ga ions impinging on the surface indeed sputter away material from the sample surface this means that the final surface of the sample after reconditioning has not experienced the complete Ga ion dose. It is therefore likely that the actual amount of damage and implantation is lower than that calculated using TRIM.

The calculations performed above should be compared to the estimated EBSD interaction depth (the sample depth from where backscattered Kikuchi patterns are generated). The interaction volume during EBSD analyses is difficult to determine exactly but it has been studied in the past [19,20,21,22,23]. In summary, the effective resolution in the longitudinal direction can be estimated

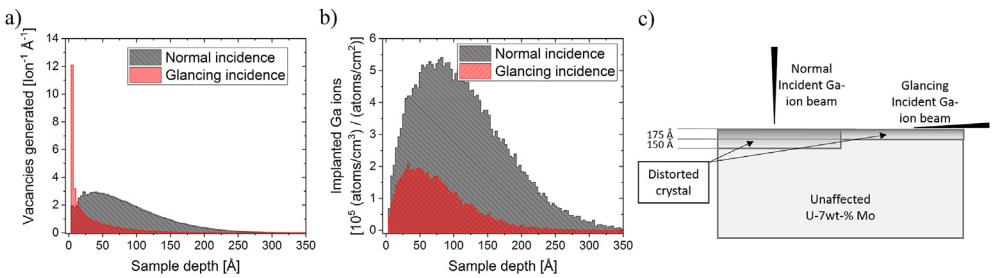

Fig. 4. TRIM calculations showing the a) total vacancies generated for ions impinging on the sample surface and b) implanted Ga ions as a function of sample depth at glancing and normal angle, respectively. c) Illustration of the damage depth calculated in a) and b).

to be three times the lateral resolution due to the high electron beam to sample tilt angle during EBSD measurement, as shown in Fig. 2b for definitions. No EBSD interaction volume data have been published for a high-density material like U-7 wt% Mo but it is estimated that the lateral resolution is around 40 nm for the current experimental settings. Several values for the effective depth resolution have been reported in the literature. One study that is relevant to the present work is the work by Wisniewski et al. [22]. They reported that correct indexing of cubic Si was possible through a 142 nm thick amorphous Si layer using similar experimental condition as in the present work. The analogy to this work is illustrated in Fig. 4c. In the present work, it was possible to index Kikuchi patterns correctly through a 20-nm-thick distorted layer after polishing the surface with gracing incidence Ga ions while no Kikuchi patterns were generated if a 40-nm-thick distorted layer formed using normal incidence ions. This results in that the depth resolution should be better than 40 nm during EBSD measurements using an electron acceleration voltage of 30 kV on a U-7 wt% Mo sample.

SEM micrographs from the unirradiated (JJ-652) and irradiated (KGT-2141) samples, after surface polishing using Ga ions at glancing angle, are shown in Fig. 5a and b, respectively. The Ga ions impinge on the sample surface from the lower part of the micrographs, and the surface polishing using the FIB results in the so called curtaining effect showing up as linear features elongated parallel to the ion beam direction. This is a result of an uneven sample surface leading to uneven removal of material from the sample surface. This effect is further enhanced in the irradiated sample where fission bubbles are present. If the curtaining introduced produces steep edges in the sample and the beam hits in the valley the resulting Kikuchi pattern will be shadowed by the samples itself (the edges of the curtains). It is thus important to keep the curtaining effect as small as possible. The resulting curtains observed in Fig. 5 could be tolerated as they did not produce shadowing to the EBSD detector.

3.2. Electron backscatter diffraction measurements

Inverse pole figure maps from EBSD measurements are shown in Fig. 6. The step size used in the maps is 50 nm, and is therefore also the resolution limit in the maps. The average confidence index was above 0.4–0.5 for this work, which is satisfactory considering that, at a confidence index of 0.1, 99.5% of patterns are indexed correctly. The black regions in the inverse pole figure maps are non-indexed points. Non-indexed points result when the acquired Kikuchi pattern data cannot be indexed. This can be observed in the edges of the unirradiated sample fuel particle, especially in the top part. It is also very prominent in the inverse pole figure for the irradiated sample. However, the reason for the non-indexed points is different in the two cases. The non-indexed points in the unirradiated map is most probably due to defects in the surface layer while the majority of the non-indexed points in the irradiated sample are due to bubbles/voids present in the interaction volume of the electron beam during the EBSD measurement. These features are a part of the samples and should not be considered artificial. These bubbles have formed as a result of gas generation from uranium fissions and subsequent nucleation and growth of fission gas bubbles. No standard data clean-up routines, commonly used during EBSD data evaluation, were employed for these maps, but offline Kikuchi pattern re-indexing using the Neighbor Pattern Averaging and Reindexing (NPAR) routine was applied [18]. Although this routine will not alter the collected data, it may slightly decrease the spatial resolution. Furthermore, it is clear that the bubbles that form during irradiation affect the measurements not only when intersecting on the sample surface but also when they are very close to the surface, see black regions in the inverse pole figure map of the irradiated fuel sample. The results shown in this section was reproduced analyzing other fuel particles and should be considered representative for these materials.

The grains in the as-fabricated fuel particle are both equiaxed and columnar morphology. A cellular structure with alternating concentrations of Mo, as reported in Ref. [12], could not be revealed. No elemental analyses were performed in this work but it is clear that if the cellular structure is present in this material it does not affect the crystal structure or orientation. Most grains seem to be fully recrystallized γ-(U,Mo) phase with very little intragranular misorientation (varying color in the inverse pole figure maps within the grain) that would indicate residual strain. Some of the large grains in the outer part of the particle do show intragranular misorientation indicating some residual strain, possibly due to a locally different cooling rate from final heat treatment of fuel fabrication.

Molybdenum depletion in the grain boundaries leading to the formation of α-U has been observed previously but this could not be observed with confidence in this work. The phase map in Fig. 7 indicates the presence of α-U phase in the grain boundaries from the center region of Fig. 6a but this is most probably just an artifact of that the Kikuchi patterns close to grain boundaries may contain intensity from two different grains. This may lead to that the Kikuchi pattern is falsely indexed as the wrong phase.

In fact, the observation that the phase map shows a thicker false grain boundary α-U phase for grain boundaries extending in the lateral direction (2–3 steps, 100–150 nm) compared to that in the longitudinal direction (0–1 steps, 0–50 nm) suggest that this would correspond to the resolution limit during the measurements. These values for the resolution correspond well to that described in

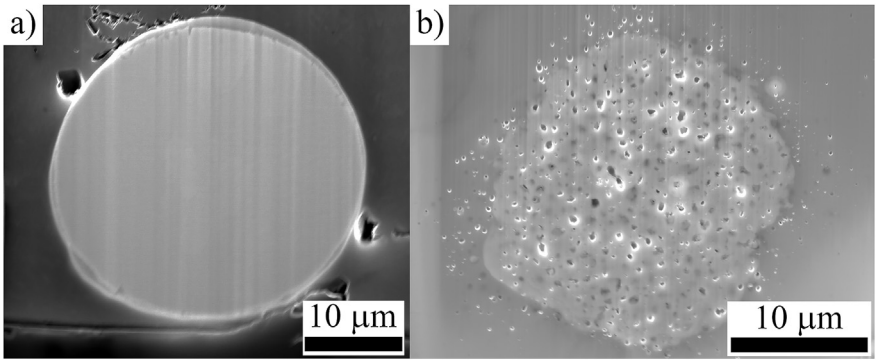

Fig. 5. Secondary electron SEM micrographs of the a) unirradiated and b) irradiated U-7 wt% Mo dispersion fuel sample after surface polishing using the FIB.

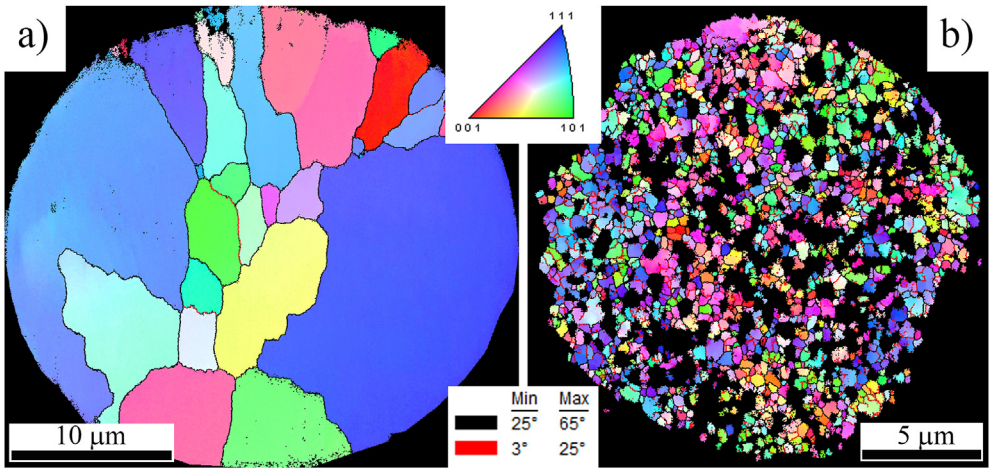

Fig. 6. Overview inverse pole figure EBSD measurements from a) the unirradiated sample showing the grain texture of U-7 wt% Mo particle in as-fabricated fuel and b) the irradiated U-7 wt% Mo sample showing grain subdivision resulting from irradiation. Red: Low angle and Black: High angle grain boundaries. The black regions in the maps for the irradiated sample correspond to bubbles/voids in the material. (For interpretation of the references to color in this figure legend, the reader is referred to the Web version of this article.)

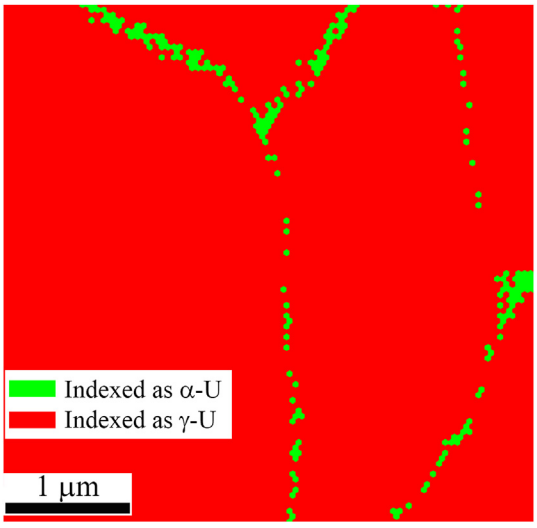

Fig. 7. EBSD phase map from the unirradiated samples indicating the presence of α-U phase at grain boundaries. However, this is most probably due to overlapping Kikuchi patterns originating from each side of the γ-U grain boundary.

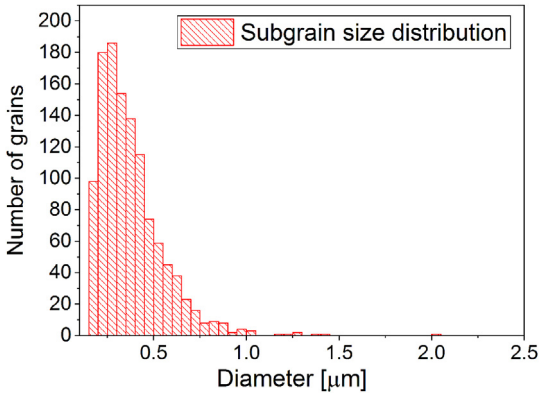

Fig. 8. Subgrain size distribution for the irradiated sample KGT-2141 based on measuring the size of 1576 subgrains.

the previous section about spatial resolution of EBSD in this work.

The microstructure of the irradiated fuel particle clearly shows that subgrain formation has occurred during irradiation. The original large grains are subdivided into small sub-micron sized and equiaxed grains and cover the whole analyzed region. As described in [14], subgrains start to form at a fission density of around 3×10^{21} fissions/cm^3 and is preceded by steady state swelling due to solid fission product incorporation in the γ-U lattice. Enhanced, or break-away, swelling begins at around 5×10^{21} fissions/cm^3 due to an accelerated growth of large fission gas bubbles with a completely restructured grain structure. These values are in agreement with what is observed in the present work.

The equivalent grain size diameter calculated from the EBSD measurements is ~4 μm for the as-fabricated fuel particle while the grain size for the irradiated particle is ~0.3 μm, as shown in Fig. 8. Although a grain size diameter lower cut-off was made at 100 nm due to the resolution limit of the measurements this value is still representative of the true grain size for the subdivided grain structure. The grain boundary characteristics also change from being mainly high angle grain boundaries (95%, >15° GB angle) in fresh U-7 wt% Mo fuel to low angle grain boundaries (55%, <15° GB angle) in irradiated U-7 wt% Mo fuel.

The mechanism for subgrain formation could be either polygonization or recrystallization. Polygonization would involve annihilation of defects and rearrangement of dislocations to form a low angle grain boundary and recrystallization would produce high angle grain boundaries and grains that are free from defects. Recrystallization could be driven by the stored energy in form of defects but also by the fission products in solid solution. The detailed EBSD inverse pole figure map in Fig. 9 shows low angle (<15°) and high angle (>15°) grain boundaries in red and yellow, respectively. It is clear that most of the subgrain boundaries are low angle boundaries supporting the hypothesis that polygonization is the mechanism for subgrain formation during irradiation of these U-7 wt% Mo fuel particles. Many of the subgrains also show intragranular misorientation indicative of the presence of geometrically necessary dislocation, i.e. residual strain, further supporting this statement. The encircled region in Fig. 9 contains almost only low angle grain boundaries. It is thus likely that this region was once a large grain similar to the grains observed in the unirradiated sample. Black arrows point to locations where incomplete grain boundaries can be observed. This indicates the process of subgrain

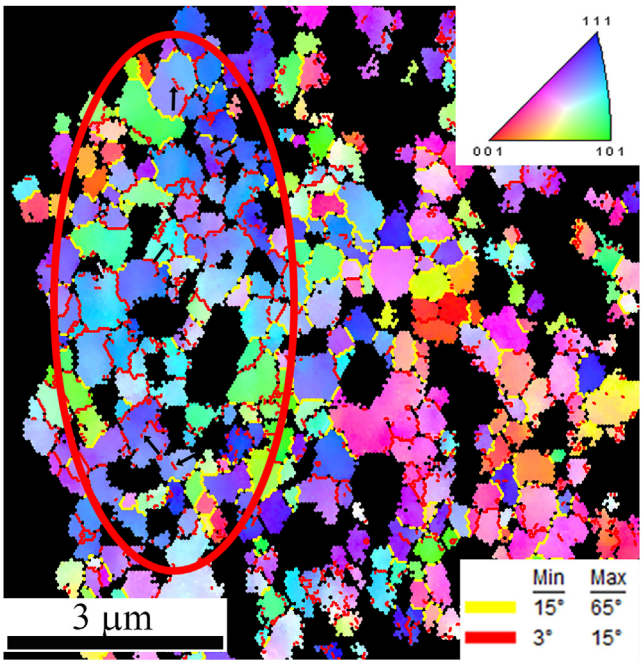

Fig. 9. EBSD inverse pole figure map showing the subgrain structure of the irradiated fuel particle in detail. Arrows show incomplete grain boundaries. Black regions are areas that could not be indexed and mainly corresponds to bubbles and pores in the material.

formation was still on-going when the fuel plate was taken out of the reactor. The formation of predominantly low angle grain boundaries is not compatible with the nucleation and growth required for recrystallization to be the mechanism behind the subgrain formation.

Fig. 10 shows EBSD texture plots and grain boundary texture plots for both as-fabricated and irradiated material. It should be noted that the amount of grains is insufficient to illustrate the texture of a material, particularly for the unirradiated sample, and these plots are only used in this work to illustrate the difference in the orientation of the grains before and after irradiation. After irradiation it can be observed that the pole angular spreads are larger than before irradiation. This is consistent with the observation above that low angles grain boundaries are formed increasing the diversity in grain orientation after subgrain formation. The subgrains do not have a completely random orientation. These observations supports polygonization as the active mechanism for subgrain formation. The grain boundary texture plots are illustrating the same thing as discussed above. The unirradiated sample contains mainly high angle grain boundaries and there is a shift towards lower angle boundaries for the irradiated sample.

Grain subdivision of irradiated U-Mo fuel into the small grains (100–300 nm) at fission densities higher than 3×10^{21} fissions/cm^3 was also reported from the previous transmission electron microscopy (TEM) characterization by Gan et al. for both dispersion and monolithic fuels [24,25]. The subdivided grains have small misfit angles which cannot be resolved in early conventional scanning electron microscopy micrographs due to technical difficulty on sample surface finish for the highly radioactive irradiated fuel. The current EBSD result are consistent with that of previous TEM characterizations but with significantly improved statistics because the entire cross section of a fuel particle is analyzed with the total number of subdivided grains significantly higher than that accessible to TEM analysis. Spino discussed that the term recrystallization is used to indicate grain refinement or grain subdivision

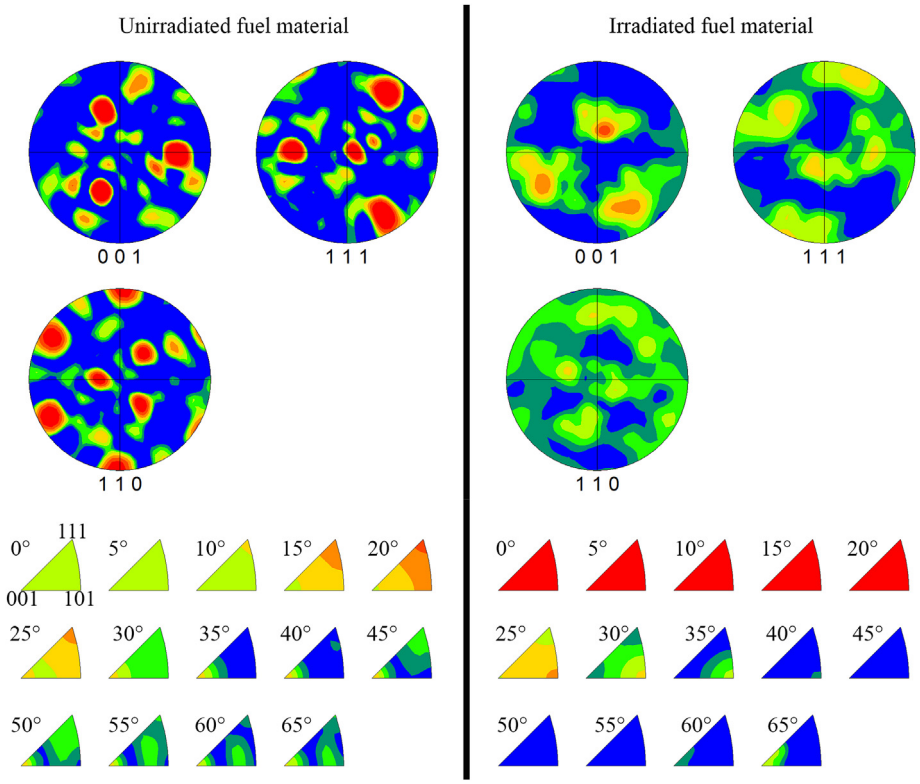

Fig. 10. EBSD texture plots (upper row) and grain boundary texture plots (lower row) for both the unirradiated and irradiated U-Mo samples. The color scale is the same for both samples to enable a one to one comparison. The legend is the same for all color coded grain boundary plots. Green: low intensity, red: high intensity. (For interpretation of the references to color in this figure legend, the reader is referred to the Web version of this article.)

without the meaning that this process has to be understood in the classical sense of metallurgy, namely as a consequence of intense cold-working and annealing [26]. While the term polygonization seems a more accurate description of the grain subdivision in irradiated U-Mo fuel, the continuing use of term recrystallization seems unnecessary and, to a certain extent, could be misleading.

4. Conclusions

In summary, FIB in-situ glancing angle ion polishing is an effective tool for preparing the surface of un-irradiated and as-irradiated U-Mo fuel alloy for high quality EBSD characterization. The unirradiated U-7 wt% Mo fuel particle consists of large grains (~4.0 μm) and high angle grain boundaries. For irradiated U-7 wt% Mo at a fission density of 5.3×10^{21} fissions/cm^3, the original large grain is subdivided into thousands of smaller grains (~0.3 μm) and most of these subdivided grain boundaries are low angle boundaries. The EBSD analysis suggests that the grain subdivision in the irradiated U-7 wt% Mo was driven by polygonization, not recrystallization.

5. Declarations of interest

None.

Acknowledgements

Staff at the Electron Microscopy Laboratory at Idaho National Laboratory's Materials and Fuels Complex are gratefully acknowledged for support throughout this work. Furthermore, this work was supported by the United States Department of Energy, Office of Materials Management and Minimization, National Nuclear Security Administration, under DOE-Idaho Operations Office Contract DE-AC07-05ID14517. This manuscript was authored by a contractor for the U.S. Government. The publisher, by accepting the article for publication, acknowledges that the US Government retains a nonexclusive, paid-up, irrevocable, worldwide license to publish or reproduce the published form of this manuscript, or allow others to do so, for US Government purposes.

Appendix A. Supplementary data

Supplementary data related to this article can be found at https://doi.org/10.1016/j.jnucmat.2018.06.007.

References

[1] J.L. Snelgrove, G.L. Hofman, M.K. Meyer, C.L. Trybus, T.C. Wiencek, Nucl. Eng. Des 178 (1997) 119–126.
[2] D.D. Keiser Jr., S.L. Hayes, M.K. Meyer, C.R. Clark, JOM 55 (9) (2003) 55–58.
[3] M.K. Meyer, G.L. Hofman, S.L. Hayes, C.R. Clark, T.C. Wiencek, J. Nucl. Mater 304 (2002) 221–236.
[4] C.A.W. Peterson, W.J. Steele, S.L. DiGiallonardo, Isothermal Transformation Study of Some Uranium-base Alloys, UCRL-7824 Report, University of California, 1964.
[5] M.K. Meyer, C.L. Trybus, G.L. Hofman, S.M. Frank, T.C. Wiencek, Selection of microstructures of high density uranium alloys, in: The 20th RERTR Conference, Jackson Hole, WY, Oct. 5-10, 1997.
[6] G.L. Hofman, Y.S. Kim, H.J. Ryu, J. Rest, D.M. Wachs, M.R. Finlay, Attemp to solve the instability in the irradiation behavior of low enriched U-Mo/Al dispersion fuel, in: Transaction of the 10th Research Reactor Fuel Management Conference (RRFM), Sofia, Bulgaria, Apr. 30-May 3, 2006.
[7] Y.S. Kim, G. Hofman, A.B. Robinson, Effect of addition in Al in U-Mo/Al diepseraion plates: Observations from side-by-side irradiations from RERTR-6, -7A, -9A and -9B, in: Transactions of the 13th topical meeting on Research Reactor Fuel Management (RRFM), Vienna, Austria, Mar. 22-25, 2009.
[8] B. D. Miller, PhD Thesis, University of Wisconsin-Madison, 2010.
[9] A. Leenaers, UGENT/SCK-CEN, PhD thesis, 2014. ISBN-9789076971223.
[10] D.M. Wachs, A.B. Robinson, F.J. Rice, N.C. Kraft, S.C. Taylor, M. Lillo, N. Woolstenhulme, G.A. Roth, J. Nucl. Mater 476 (2016) 270–292.
[11] D. Jadernas, P. Tejland, Microsc. Microanal 20 (Suppl 3) (2014).
[12] X. Iltis, I. Zacharie-Aubrun, H.J. Ryu, J.M. Park, A. Leenaers, A.M. Yacout, D.D. Keiser, F. Vanni, B. Stepnik, T. Blay, N. Tarisien, C. Tanguy, H. Palancher, J. Nucl. Mater 495 (2017) 249–266.
[13] R.J. McCabe, A.M. Kelly, A.J. Clarke, R.D. Field, H.R. Wenk, Electron backscatter diffraction (EBSD) characterization of uranium and uranium alloys, Microsc. Microanal. 18 (Suppl. 2) (2012).
[14] A. Leenaers, W. Van Renterghem, S. Van den Berghe, JNM 476 (2016) 218–230.
[15] M.J. Nilles, J.W. Wight, Fabrication of MTR-sized high loaded dispersion fuel plates, in: Proceedings of the 30th International on Reduced Enrichment for Research and Test Reactors, 2008. Washington D.C. October 5-9.
[16] J.F. Ziegler, M.D. Ziegler, J.P. Biersack, SRIM - The stopping and range of ions in matter, Nucl. Instrum. Meth. B268 (2010) 1818–1823.
[17] R.E. Stoller, M.B. Toloczko, G.S. Was, A.G. Certain, S. Dwaraknath, F.A. Garner, Nucl. Instr. Meth. Phys. Res. B 310 (2013) 75–80.
[18] I. Stuart, M. Wright Matthew, P. Nowell Scott, P. Lindeman Patrick, A. Camus Marc De Graef Michael, Jackson Ultramicroscopy 159 (1) (December 2015) 81–94.
[19] C.J. Harland, J.H. Klein, P. Akhter, J.A. Venables, Electron back-scattering patterns in a field emission gun scanning electron microscope, in: Proc. 9th Int. Cong. on 'Electron Microscopy', Toronto, Ont., Canada, Microscopical Society of Canada, August 1978, pp. 564–565.
[20] T.C. Isabell, V.P. Dravid, Ultramicroscopy 67 (1997) 59–68.
[21] F.J. Humphreys, Journal of Material Science 36 (2001) 3833–3854.
[22] W. Wisniewski, S. Saager, A. Böbenroth, C. Rüssel, Ultramicroscopy 173 (February 2017) 1–9.
[23] S. Zaefferer, Ultramicroscopy 107 (2007) 254–266.
[24] J. Gan, D.D. Keiser Jr., B.D. Miller, A.B. Robinson, J.F. Jue, P. Medeved, D.M. Wachs, J. Nucl. Mater 424 (2012) 43–50.
[25] J. Gan, B.D. Miller, D.D. Keiser Jr., J.F. Jue, J.W. Madden, A.B. Robinson, H. Ozaltun, G. Moore, M.K. Meyer, J. Nucl. Mater 492 (2017) 195–203.
[26] J. Spino, K. Vennix, M. Coquerelle, J. Nucl. Mater 231 (1996) 179–190.